J. Plasma Phys. (2023), *vol*. 89, 905890201
Published by Cambridge University Press

doi:10.1017/S0022377823000090

Role of the overshoot in the shock self-organization

Michael Gedalin[1],†, **Andrew P. Dimmock**[2], **Christopher T. Russell**[3], **Nikolai V. Pogorelov**[4] **and Vadim Roytershteyn**[5]

[1]Department of Physics, Ben-Gurion University of the Negev, Beer-Sheva, Israel

[2]Swedish Institute of Space Physics, Uppsala, Sweden

[3]Department of Earth, Planetary, and Space Sciences, University of California, Los Angeles, CA, USA

[4]Center for Space Plasma and Aeronomic Research, The University of Alabama Huntsville, AL 35805, USA

[5]Space Science Institute, Boulder, CO 80301, USA

(Received 26 October 2022; revised 17 January 2023; accepted 18 January 2023)

A collisionless shock is a self-organized structure where fields and particle distributions are mutually adjusted to ensure a stable mass, momentum and energy transfer from the upstream to the downstream region. This adjustment may involve rippling, reformation or whatever else is needed to maintain the shock. The fields inside the shock front are produced due to the motion of charged particles, which is in turn governed by the fields. The overshoot arises due to the deceleration of the ion flow by the increasing magnetic field, so that the drop of the dynamic pressure should be compensated by the increase of the magnetic pressure. The role of the overshoot is to regulate ion reflection, thus properly adjusting the downstream ion temperature and kinetic pressure and also speeding up the collisionless relaxation and reducing the anisotropy of the eventually gyrotropized distributions.

Key words: space plasma physics, plasma heating, astrophysical plasmas

1. Introduction

Collisionless shocks are among the most fundamental and ubiquitous phenomena in plasmas. The vast majority of these shocks are fast shocks in a magnetized electron–ion plasma. Such shocks are formed in laboratory set-ups (Kurtmullaev *et al.* 1966; Eselevich *et al.* 1971; Niemann *et al.* 2014; Schaeffer *et al.* 2017; Fiuza *et al.* 2020; Yao *et al.* 2022) and their activity is observed in clusters of galaxies (Medvedev, Silva & Kamionkowski 2006; Simionescu *et al.* 2009; Iapichino & Brüggen 2012). Energy redistribution is the central problem of the shock physics. Since energy is frame dependent, the forthcoming discussion will be carried out either in the normal incidence frame (NIF) or in the de Hoffman–Teller frame (HT). Both refer to the magnetohydrodynamic (MHD) shock

† Email address for correspondence: gedalin@bgu.ac.il

description which treats a shock as a planar stationary discontinuity between the uniform upstream and downstream states. In NIF the upstream plasma flow is along the shock normal, whereas in HT the plasma flow is along the magnetic field in both asymptotic regions. Let B_u be the upstream magnetic field magnitude, V_u be the upstream flow speed in NIF and m_i be the ion mass. The dominant ion species in most space plasmas is protons. The MHD approach is valid on the scales substantially exceeding the upstream convective gyroradius, $\rho_i = V_u/\Omega_u$, where $\Omega_u = eB_u/m_ic$ is the upstream ion gyrofrequency. In this approach, the role of a shock is abrupt transfer of the conserved quantities, i.e. mass, momentum and energy, from the upstream region to the downstream region. Real shocks are well-structured and multi-scale self-organized systems. Self-organization means that even if the microprocesses in the shock transition are not known, the eventual result of these processes would be the above mentioned stable transfer. Detailed knowledge of the processes leading to maintenance of a shock as an MHD formation requires simultaneous solution of the kinetic equations (or equations of particle motion, which is the same) for all species and of the Maxwell equations. At present, this is hardly possible analytically, even if restricting the task to ions only. Self-consistent numerical simulations, which strive to reproduce nature on a computer, are among the most powerful and important tools (see, e.g. for some recent studies and more references Krasnoselskikh *et al.* 2002; Burgess *et al.* 2016; Haggerty, Bret & Caprioli 2021; Omidi *et al.* 2021; Wilson, Chen & Roytershteyn 2021). Self-consistency is both the strength and the weakness of such simulations. On the one hand, by fixing a limited number of basic shock parameters, i.e. the Mach number, the shock angle and the upstream temperature, all other details, like the shock width and cross-shock potential, are obtained during the evolution. On the other hand, all the interactions between the charged particles and fields remain entangled, and the problem of analysis remains intact. For example, it is not possible to have a shock without an overshoot and another one with an overshoot for the same upstream conditions. Thus, it is not possible to compare the ion distributions which would be obtained without overshoot, if the latter appears in a self-consistent way.

The only place where the physical processes in the shock transition can be studied with *in situ* measurements is the heliosphere. More than six decades of the Earth bow shock, planetary bow shocks and interplanetary shock studies has shown that a collisionless shock is a well structured and multi-scale system. The structure becomes progressively more complex with the increase of the fast magnetosonic Mach number, M_f. Note that the Alfvénic Mach number, which is used throughout this paper and is denoted M hereafter, is always larger than the fast Mach number. The magnetic profile of a low Mach number, low-β shock has a simple ramp and possibly weak overshoot (see, e.g. Farris, Russell & Thomsen 1993). The subscript u denotes upstream, $\beta = 8\pi n_u T_u/B_u^2$ is the ratio of the thermal-to-magnetic pressure, n_u is the upstream number density and T_u is the upstream temperature. At higher Mach numbers, overshoots and subsequent downstream magnetic oscillations are stronger, and a foot is developed ahead of the ramp (see, e.g. Krasnoselskikh *et al.* 2013). In addition, the shock front may become non-planar (rippled) and/or time dependent (see, e.g. Lowe & Burgess 2003), or possibly reforming (see, e.g. Krasnoselskikh *et al.* 2013). We consider all these as a structure of the macroscopic fields in the shock front. In addition, there are smaller-scale fluctuations, coherent or random, which also affect the particle motion. The present state of art observations of the Earth bow shock by the Magnetospheric Multiscale Mission (MMS) (Burch *et al.* 2016) provide high resolutions measurements of the fields and particles (Pollock *et al.* 2016; Russell *et al.* 2016) by four spacecraft. Yet, each spacecraft measures only along its path, and even four spacecraft are unable to provide information about the state of the plasma in all points of even a limited region.

https://doi.org/10.1017/S0022377823000090 Published online by Cambridge University Press

Given the above mentioned limitations of theory, simulations and observations, a viable approach would be to study separately and not self-consistently the effect of charged particles on the shock structure, and separately and not self-consistently the effect of the shock fields on the particle dynamics. After both influences are understood sufficiently well, they may be combined to achieve a desired level of self-consistency to be further compared with simulations and observations. At present, a theoretical description of the formation of the overshoot, undershoot and additional coherent downstream magnetic oscillations due to the post-ramp ion gyration is developed (Balikhin *et al.* 2008; Ofman *et al.* 2009) and successfully confirmed with observations on low Mach number shocks (Pope, Gedalin & Balikhin 2019; Pope 2020). According to this theory, the variations of the magnetic pressure arise as a response to the variations of the dynamic and kinetic ion pressures as a result of the required momentum conservation throughout the shock front. The latter means that the momentum flux, or the total pressure, should be constant as a function of the coordinate of along the shock normal. Upon crossing the shock front the whole ion distribution begins to gyrate, so that the total ion pressure becomes position dependent. This dependence is gradually smoothed out due to the gyrophase mixing. The same one-dimensional time-independent physics is shown to be approximately valid for moderately supercritical shocks (Gedalin 2019*a*,*b*). In rippled shocks the momentum conservation should be modified to include time dependence and spatial dependence along the shock front (Gedalin & Ganushkina 2022). Yet, the conservation laws are valid, and the variations of fluxes belonging to particles should be compensated by variations of the fluxes due to the fields. We suggest that a collisionless shock may be considered as self-organized systems. The main task of a collisionless shock is to ensure prompt and stable transfer of the conserved quantities (mass, momentum and energy) from one region (upstream) to another region (downstream). The transfer of these quantities in the shock is accompanied by entropy production. By 'prompt' we mean that a collisionless shock transition is too narrow to be treated within MHD. By 'stable' we mean that there are no disruptions or substantial changes on average, except those which are caused by variations of ambient conditions. In this approach the developing shock structure is the one which ensures this transfer. The proposed approach shifts the focus from reason to purpose: the shock structure is considered according to its task in maintaining stable transfer of the mass, momentum and energy. This means that, if stable transfer is not possible without an overshoot, an overshoot has to be formed. If it is not possible without rippling, rippling will develop. Since ions are the main carriers of these conserved quantities, it is ions which are responsible for developing the structure and it is ions which have to be most strongly affected by it. The main role of the shock structure is to regulate ion reflection and shape ion distributions towards consistency of the self-organized shock. In this paper we focus on quasiperpendicular shocks, for which the angle between the shock normal and the upstream magnetic field $\theta > 45^\circ$, since these shocks have a well-defined structure. The objective of the present paper is to elucidate the role of the overshoot, which is one of the main features or supercritical shocks (those in which ion reflection is significant). The structure of quasiparallel shocks may be different and requires a separate analysis. Here we consider only a planar time-independent shock profile.

2. Observational illustration

In order to illustrate what we are supposed to be able to explain, figure 1 shows the magnetic field profile and the reduced ion distribution

$$f(t, v_n) = \int F(\boldsymbol{v}, t)\, \mathrm{d}v_{t_1}\, \mathrm{d}v_{t_2}. \tag{2.1}$$

https://doi.org/10.1017/S0022377823000090 Published online by Cambridge University Press

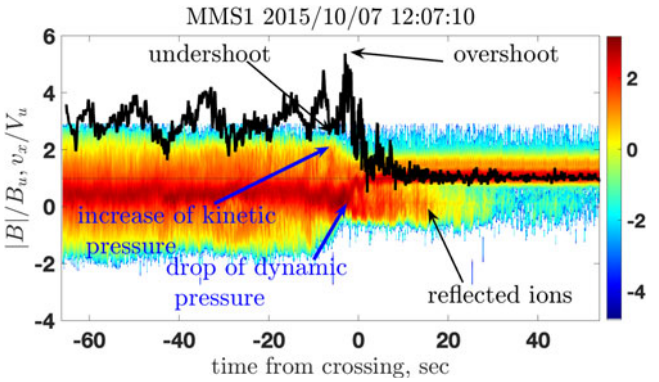

FIGURE 1. The magnetic field magnitude, normalized to the upstream magnetic field magnitude (black curve) and the reduced ion distribution function. See details in text.

Here, n denotes the direction along the shock normal, t_1, t_2 are two perpendicular directions along the shock front, and $F(\boldsymbol{v}, t)$ is the three-dimensional distribution as a function of time, measured in the spacecraft frame. The shock crossing was observed by MMS 1 on 07 October 2015 at 12:07:10 and documented in the database `https://zenodo.org/record/6343989#.Yxxbbi0Rokw` (Lalti *et al.* 2022). The model shock normal is used (Farris & Russell 1994). The listed shock parameters are: the Alfvénic Mach number $M \approx 5$, the angle between the shock normal and the upstream magnetic field $\theta \approx 70^\circ$ and $\beta_u = 0.4$. In the figure the magnetic field magnitude is normalized on the upstream magnetic field B_u, and the normal component of the ion velocity is shifted into NIF and normalized on the upstream plasma speed V_u. For the visualization the distribution is normalized on $\max f(t, v_n)$ in the whole range of the figure and plotted in the log scale. The magnetic compression $B_d/B_u \approx 3$. Here, and in what follows, u denotes upstream and d denotes downstream. Since the measurements of the cold solar wind are not very precise, the values of v_n are very approximate and the plot is for illustrative purposes only. The arrows in the figure show the main features which are expected to affect the ion motion, the overshoot and the undershoot and the population of reflected ion which is expected to be affected. One blue arrow points to the position where the dynamic pressure drops while the kinetic pressure is not large yet. This is the position of the overshoot, that is, the point where the magnetic pressure is maximum. The second blue arrow points to the position where the kinetic pressure is maximum, this point corresponds to the undershoot. These conclusions follow from the approximate constancy of the total pressure across the shock (Gedalin 2019*a*,*b*).

3. Overshoot and ion reflection

Ion reflection in the shock front occurs due to the combined influence of the electric and magnetic fields. In order to elucidate the effect of both let us consider the motion of an ion entering the ramp. The most part of the magnetic field jump occurs from the beginning of the ramp to the maximum of the overshoot. This is also the region where the cross-shock electric field acts. Let the shock normal be in the x direction and the upstream magnetic field reside in the $x - z$ plane. The equations of motion for the ion inside the

https://doi.org/10.1017/S0022377823000090 Published online by Cambridge University Press

ramp-overshoot region are

$$\frac{\mathrm{d}v_x}{\mathrm{d}t} = \frac{e}{m_i}E_x + \frac{e}{m_i c}(v_y B_z - v_z B_y), \tag{3.1}$$

$$\frac{\mathrm{d}v_y}{\mathrm{d}t} = \frac{e}{m_i}E_y + \frac{e}{m_i c}(v_z B_x - v_x B_z), \tag{3.2}$$

$$\frac{\mathrm{d}v_z}{\mathrm{d}t} = \frac{e}{m_i c}(v_x B_y - v_y B_x). \tag{3.3}$$

Here, we assume, for simplicity of the analysis, that the shock is planar and stationary. Then in NIF $E_z = 0$, $E_y = V_u B_u \sin\theta/c = \text{const.}$ and $E_x = -(\mathrm{d}\phi/\mathrm{d}x)$, where ϕ is the cross-shock potential depending on the coordinate along the shock normal. The subscript u denotes upstream and θ is the angle between the shock normal and the upstream magnetic field. At the entry to the ramp $v_{x0} - V_u$, v_{y0} and v_{z0} are of the order of the upstream thermal speed v_T. According to the observations (see, e.g. Sckopke *et al.* 1983), the incident ion distribution is usually approximated by an isotropic Maxwellian distribution. For the present analytical consideration it is not essential, v_T is just the measure of the spread in the velocity space. Upon crossing the shock the ion distribution becomes strongly non-gyrotropic and gradually gyrotropizes and isotropizes. The ratio of the thermal speed to the upstream plasma speed $v_T/V_u = \sqrt{\beta_{ui}/2}/M$ and decreases with the increase of the Mach number. An ion is reflected if at some x the ion velocity $v_x = 0$. Up to this point $v_x > 0$ and we may replace $(\mathrm{d}/\mathrm{d}t) = v_x(\mathrm{d}/\mathrm{d}x)$ and integrate (3.1)–(3.3) from the entry to the ramp, x_0, to the reflection point x_r, as follows:

$$-\frac{1}{2}v_{x0}^2 = \frac{e}{m_i}\int_{x_0}^{x_r} E_x\,\mathrm{d}x + \frac{e}{m_i c_i}\int_{x_0}^{x_r}(v_y B_z - v_z B_y)\mathrm{d}x, \tag{3.4}$$

$$v_y - v_{y0} = \frac{e}{m_i c}\int_{x_0}^{x_r}\left(\frac{B_u \sin\theta V_u}{v_x} - B_z\right)\mathrm{d}x + \frac{e}{m_i c}\int_{x_0}^{x_r}\left(\frac{v_z B_x}{v_x}\right)\mathrm{d}x, \tag{3.5}$$

$$v_z - v_{z0} = \frac{e}{m_i c}\int_{x_0}^{x_r}\left(B_y - \frac{v_y B_x}{v_x}\right)\mathrm{d}x, \tag{3.6}$$

or

$$\frac{1}{2}v_{x0}^2 = \frac{e}{m_i}\phi(x_r) - \frac{e}{m_i c}\int_{x_0}^{x_r}(v_y B_z - v_z B_y)\,\mathrm{d}x. \tag{3.7}$$

In the right-hand side of this expression v_y, v_z, B_y, B_z depend on x, so that the integral cannot be calculated exactly but can be estimated. The width of the ramp itself is of the order of the ion inertial length or smaller. The distance from the beginning of the ramp to the overshoot maximum is substantially smaller than the ion convective gyroradius V_u/Ω_u. Thus, the narrow transition approximation would be appropriate. In the expressions for v_y and v_z the component v_x is of the order of V_u throughout, so that the variations of v_y and v_z are proportional to the width and may be neglected in (3.7). Since the ion starts at the point where $B_y = 0$, the lowest-order estimate would be

$$\frac{m_i}{2}v_x^2 = \frac{m_i}{2}v_{x0}^2 - e\phi_{\mathrm{eff}}, \tag{3.8}$$

$$\phi_{\mathrm{eff}} = \phi(x_r) - \frac{1}{c}v_{y0}\int_{x_0}^{x_r} B_z\,\mathrm{d}x. \tag{3.9}$$

https://doi.org/10.1017/S0022377823000090 Published online by Cambridge University Press

At the reflection point $v_x = 0$ and therefore

$$\frac{m_i v_{x0}^2}{2} = e\phi_{\rm eff}, \quad v_{x0} = \sqrt{\frac{2e\phi_{\rm eff}}{m_i}}, \tag{3.10a,b}$$

which gives

$$\frac{V_u - v_{x0}}{v_T} = \frac{M\left(1 - \sqrt{\dfrac{2e\phi_{\rm eff}}{m_i V_u^2}}\right)}{\sqrt{\beta_{ui}/2}}. \tag{3.11}$$

If the magnetic breaking is not taken into account $\phi_{\rm eff} = \phi \sim 0.5(m_i V_u^2/2e)$ (Morse 1973; Schwartz *et al.* 1988; Dimmock *et al.* 2012). For typical $\beta \sim 1$ (Farris *et al.* 1993) and $M = 4$ the ratio (3.11) is > 1.6. That is, the reflected ions come from the tail of the incident distribution. The number of these reflected ions should be small, but even a modest increase of the effective potential may result in a significant increase of the number of reflected ions. The addition to the effective potential (3.9) due to the magnetic braking (the second term on the right-hand side) can be estimated as follows:

$$v_{y0}\int_{x_0}^{x_r} B_z\,{\rm d}x \sim v_T B_{\rm max} L, \tag{3.12}$$

where $B_{\rm max}$ is the maximum magnetic field in the ramp-overshoot region and L is the distance from the entry to the ramp to this maximum. Without an overshoot, $B_{\rm max} = B_d$, and L is the ramp width, which is of the order of the ion inertial length or smaller (Newbury, Russell & Gedalin 1998; Hobara *et al.* 2010). With the overshoot $B_{\rm max}$ may be substantially larger than B_d, and L may be of the order of the upstream ion convective gyroradius (Bale *et al.* 2003, 2005; Krasnoselskikh *et al.* 2013). Thus, the contribution of the overshoot to the effective potential is significant and its presence should enhance ion reflection.

4. Model

The objective of this study is to understand what the effects of the overshoot and undershoot are. Since there is no hope of solving the equations of motion analytically, we will perform a test particle analysis in a model shock profile. We are not going to reproduce the observed profile and distributions, especially when some important parameters, like the shock width and the cross-shock potential, are either not known or cannot be determined with the precision required for quantitative comparison. We therefore choose a shock model, that is, the electric and magnetic fields, and trace ions in these fields. Tracing is done in NIF. Although at the Mach number of $M \approx 5$ the shock can be expected to be rippled, we ignore here possible deviations from planarity and time dependence. In what follows all fields depend only on one coordinate, x, which is the direction of the shock normal, pointing toward downstream, by definition. The non-coplanarity direction is y. In the analysis we use the normalized variables $\boldsymbol{B}/B_u$, $\boldsymbol{v}/V_u$, $c\boldsymbol{E}/V_u B_u$, $\Omega_u x/V_u$ and $\Omega_u t$ without changing the notation. The basic profile is given by

$$B_x = \cos\theta, \quad B_z = \frac{R+1}{2} + \frac{R-1}{2}\tanh\frac{3x}{D}, \quad B_y = C_B\frac{{\rm d}B_z}{{\rm d}x}, \tag{4.1a–c}$$

$$E_x = -C_E\frac{{\rm d}B_z}{{\rm d}x}, \quad E_y = \sin\theta, \quad E_z = 0. \tag{4.2a–c}$$

https://doi.org/10.1017/S0022377823000090 Published online by Cambridge University Press

Here, D is the ramp width in terms of the upstream convective gyroradius V_u/Ω_u, $\Omega_u = eB_u/m_ic$ is the upstream ion (proton) gyrofrequency, V_u is the upstream plasma speed in NIF and θ is the angle between the upstream magnetic field vector and the shock normal. The magnetic compression is $B_d/B_u = \sqrt{R^2 \sin^2\theta + \cos^2\theta}$. The coefficients C_B and C_E are determined from the conditions

$$-\int_{-\infty}^{\infty} E_x \,\mathrm{d}x = s_{\mathrm{NIF}}, \tag{4.3}$$

$$s_{\mathrm{NIF}} - s_{\mathrm{HT}} = \tan\theta \int_{-\infty}^{\infty} B_y \,\mathrm{d}x, \tag{4.4}$$

where $s = 2e\phi/m_iV_u^2$ is the normalized cross-shock potential. In order to avoid any temptation to compare with the observed shock we use slightly different parameters. The chosen shock angle is $\theta = 60^\circ$ and $\beta_i = 8\pi n_u T_{iu}/B_u^2 = 0.5$, where T_{iu} is the upstream ion temperature. The chosen Mach number is $M = 4$. At these shock parameters rippling is expected to be less pronounced (Ofman & Gedalin 2013), so that the planar stationary model may be expected to be a satisfactory approximation. The magnetic compression $B_d/B_u = 2.8$ is obtained from the Rankine–Hugoniot relations (see, e.g. Kennel 1988). The chosen ramp width is taken as one ion inertial length $D = 1/M$ (Newbury *et al.* 1998; Hobara *et al.* 2010), and the chosen cross-shock potentials are $s_{\mathrm{HT}} = 0.1$ and $s_{\mathrm{NIF}} = 0.35$ (Morse 1973; Schwartz *et al.* 1988; Dimmock *et al.* 2012; Cohen *et al.* 2019; Hanson *et al.* 2019; Pope *et al.* 2019; Schwartz *et al.* 2021).

Overshoot is added using

$$\delta B_z = B_1 \left(1 + \tanh\frac{3(x - x_L)}{W_L}\right)\left(1 - \tanh\frac{3(x + x_R)}{W_R}\right), \tag{4.5}$$

with the additions to B_y and E_x using the same relations as above. Note that the width of the shock including the ramp and the overshoot is of the order of the upstream ion convective gyroradius (Bale *et al.* 2003, 2005; Krasnoselskikh *et al.* 2013). Initially, Maxwellian distributed 40 000 ions were traced across the shock and the corresponding distribution functions $f(x, \boldsymbol{v})$, projections, and moments were numerically derived using the staying time method (Gedalin 2016; Gedalin, Pogorelov & Roytershteyn 2021). We shall use the one-dimensional reduced distribution

$$f(x, v_x) = \int_{-\infty}^{\infty} \mathrm{d}v_y \int_{-\infty}^{\infty} \mathrm{d}v_z f(x, \boldsymbol{v}), \tag{4.6}$$

and the two-dimensional reduced distribution integrated over a slab $x_1 < x < x_2$

$$f(v_x, v_y) = \int_{x_1}^{x_2} \mathrm{d}x \int_{-\infty}^{\infty} \mathrm{d}v_z f(x, \boldsymbol{v}). \tag{4.7}$$

Mean quantities are defined far downstream from the shock

$$\langle F(\boldsymbol{v})\rangle = \frac{\int F(\boldsymbol{v}) f(x \to \infty, \boldsymbol{v})\,\mathrm{d}^3\boldsymbol{v}}{\int f(x \to \infty, \boldsymbol{v})\,\mathrm{d}^3\boldsymbol{v}}. \tag{4.8}$$

https://doi.org/10.1017/S0022377823000090 Published online by Cambridge University Press

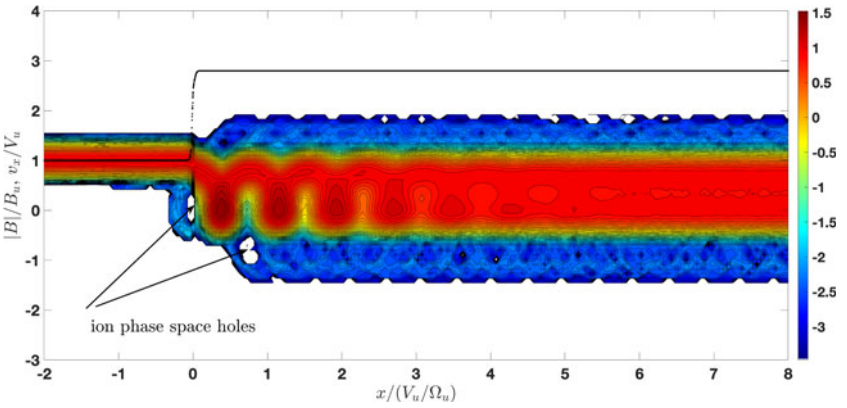

FIGURE 2. Reduced 1-D distribution $f(x, v_x)$, together with the magnetic profile.

We will be interested in the normalized parallel and perpendicular temperatures defined as follows:

$$T_\parallel = \langle((\boldsymbol{v} - \langle\boldsymbol{v}\rangle)\cdot\hat{\boldsymbol{b}})^2\rangle, \quad T_\perp = \tfrac{1}{2}\langle((\boldsymbol{v} - \langle\boldsymbol{v}\rangle)\times\hat{\boldsymbol{b}})^2\rangle, \tag{4.9}$$

where $\hat{\boldsymbol{b}}$ is the direction of the downstream magnetic field. The temperatures are normalized on $m_i V_u^2$.

5. Ion distributions

We start with the basic profile without an overshoot. Figure 2 shows the one-dimensional (1-D) reduced distribution $f(x, v_x)$. There is weak ion reflection. The gyration of the downstream distribution as a whole is clearly seen, as well as the gradual gyrophase mixing. Ion phase space holes are quite pronounced. Figure 3 shows the 2-D reduced distribution integrated over the slab $1.5 < x < 1.6$. The halo of the ions which were reflected and crossed the shock again to the downstream region (hereafter 'reflected-transmitted' ions) is weak and their contribution to the downstream temperature is small. The core of the directly transmitted ions is clearly non-gyrotropic. One arrow on the plot points to the downstream drift velocity, which is approximately $V_d \approx 1/B_d$. The other one points to the maximum of the distribution ('centre'). The distance between the two in the velocity space determines the speed of gyration of the distribution as a whole and, ultimately, the amount of perpendicular heating. The parallel heating is negligible $T_{d,\parallel}/T_{u,\parallel} = 1$. The perpendicular downstream temperature is $T_{d,\perp}/m_i V_u^2 \approx 0.14$, $T_{d,\perp}/T_{u,\perp} \approx 9$ and the anisotropy is $T_{d,\parallel}/T_{d,\perp} \approx 0.11$.

We add an overshoot using (4.5) with $W_L = D$, $W_R = 3D$, $X_L = 0.5D$, $X_R = 0.5D$ and $B_1 = 1$. The maximum magnetic field is $B_m \approx 3.86$. Since the potential closely follows the magnetic profile the maximum potential at the overshoot is $s_m \approx s_{\rm NIF}(B_m/B_d) \approx 0.48$. Figure 4 shows the 1-D reduced distribution for the profile with an overshoot. There is a substantial population of reflected ions. Ion phase space holes are clearly seen. Figure 5 shows a halo of reflected-transmitted ions which contribute substantially to the downstream temperature. The core of directly transmitted ions is clearly non-gyrotropic. Ion reflection causes parallel heating $T_{d,\parallel}/T_{u,\parallel} \approx 3.87$. Perpendicular heating dominates, $T_{d,\perp}/m_i V_u^2 \approx 0.18$, $T_{d,\perp}/T_{u,\perp} \approx 11.6$. The anisotropy is weaker than in the case without overshoot, $T_{d,\parallel}/T_{d,\perp} \approx 0.33$. The higher magnetic field of the overshoot enhances ion reflection. There are more ions which are turned back before reaching the maximum of the overshoot, due to the magnetic deflection adding to the electrostatic deceleration.

https://doi.org/10.1017/S0022377823000090 Published online by Cambridge University Press

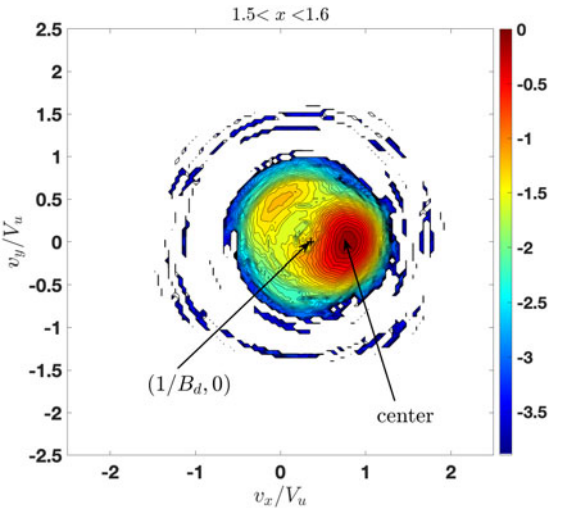

FIGURE 3. Two-dimensional reduced distribution $f(v_x, v_y)$ integrated over the slab $1.5 < x < 1.6$.

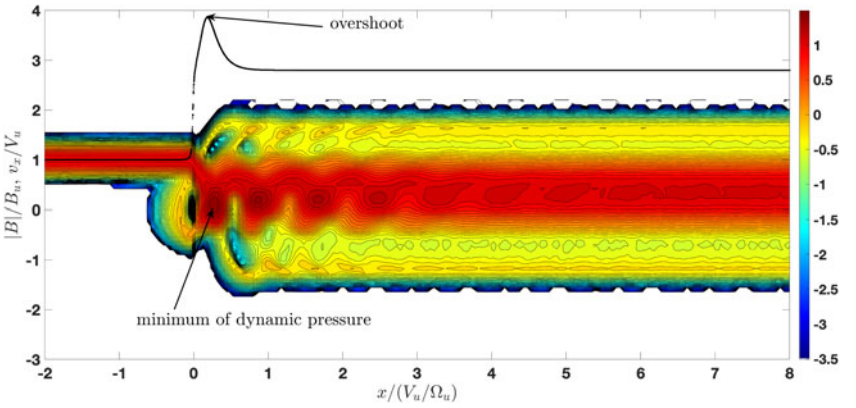

FIGURE 4. Reduced 1-D distribution $f(x, v_x)$, together with the magnetic profile.

There are more ions which turn back after crossing the maximum of the overshoot, since the drift speed is smaller and the ratio of the gyration speed to the drift speed increases. On the other hand, the higher cross-shock potential at the ramp overshoot reduces the ion velocity just after the overshoot, which reduces the gyration speed of the bulk of the directly transmitted ions and thus reduces heating of the core. This elevated potential also reduces reflection behind the overshoot.

In order to separate the effect of the potential from the effect of the magnetic overshoot, we reduce the downstream cross-shock potential to $s_{\mathrm{NIF}} = 0.25$ so that the potential at the overshoot is now $s_m \approx 0.344$. Figure 6 shows the 1-D reduced distribution for the profile with an overshoot and reduced cross-shock potential. Ion reflection is weaker but still contributes substantially to the downstream heating. Figure 7 show the corresponding 2-D reduced integrated distribution. The distance from the centre to the downstream drift speed is smaller than for the case without the overshoot but larger than for the case with overshoot and original potential. Accordingly, the core heating is larger and the relative

https://doi.org/10.1017/S0022377823000090 Published online by Cambridge University Press

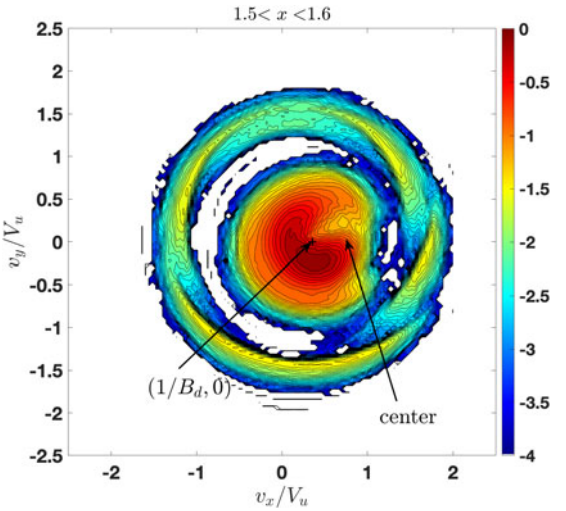

FIGURE 5. Two-dimensional reduced distribution $f(v_x, v_y)$ integrated over the slab $1.5 < x < 1.6$.

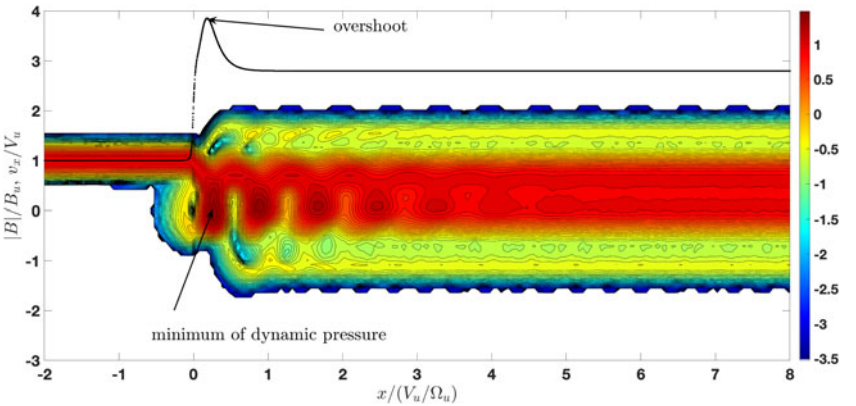

FIGURE 6. Reduced 1-D distribution $f(x, v_x)$, together with the magnetic profile.

contribution of the reflected ions is smaller. The parallel heating is noticeable, $T_{d,\parallel}/T_{u,\parallel} \approx 2.43$, because of the reflected ions. Perpendicular heating dominates, $T_{d,\perp}/m_i V_u^2 \approx 0.17$, $T_{d,\perp}/T_{u,\perp} \approx 11.18$, as in both previous cases. It is slightly weaker because of the reduced contribution of reflected ions. The anisotropy is weaker than in the case without overshoot but stronger than in the case with unreduced potential, $T_{d,\parallel}/T_{d,\perp} \approx 0.22$.

The effects of the overshoot and the potential at the overshoot are shown in figure 8. The distribution $f_d(v_\parallel, v_\perp)$ is calculated by switching to HT sufficiently far from the shock in the downstream uniform region. Here, $v_\parallel = \boldsymbol{v} \cdot \hat{\boldsymbol{b}}$ and $v_\perp = \sqrt{v^2 - v_\parallel^2}$. The heating of the core in the perpendicular direction is the largest without overshoot (left) and smallest with the overshoot and unreduced potential (middle). The heating of the core in the parallel direction is nearly the same in all cases. The overall heating, which is just the measure of the spread in the velocity space, is determined by the contribution of the reflected ions, which is the largest with the overshoot and unreduced potential and somewhat smaller for reduced potential. Without overshoot the contribution of the reflected ions is negligible.

https://doi.org/10.1017/S0022377823000090 Published online by Cambridge University Press

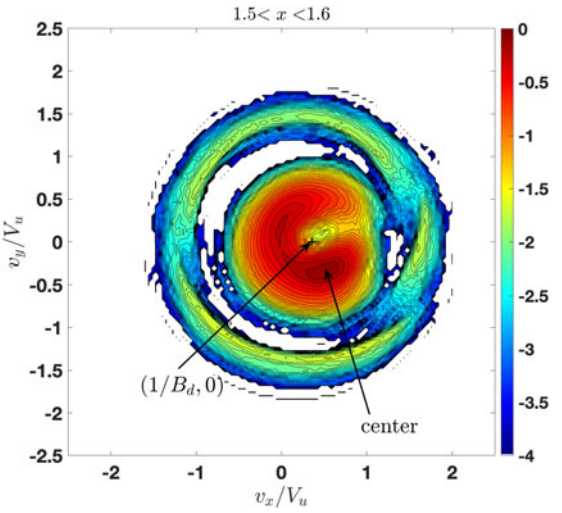

FIGURE 7. Two-dimensional reduced distribution $f(v_x, v_y)$ integrated over the slab $1.5 < x < 1.6$.

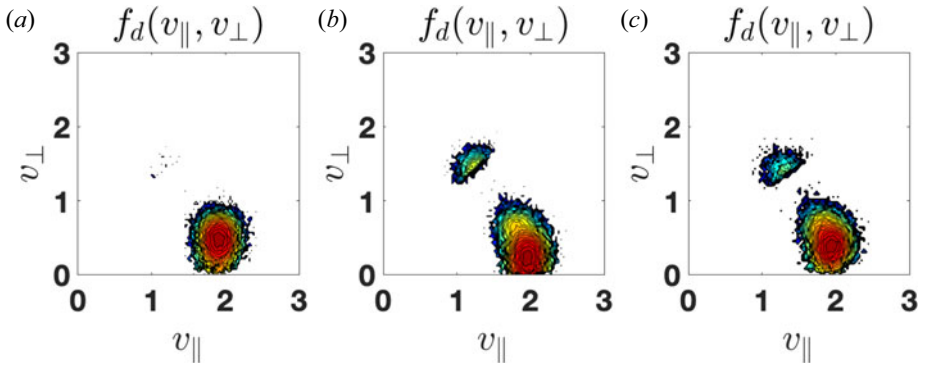

FIGURE 8. Distributions calculated in HT. (*a*) No overshoot. (*b*) Overshoot with unreduced potential. (*c*) Overshoot with reduced potential.

Figure 9 shows the total off-diagonal pressure

$$P_{xy}(x) = \int v_x v_y f(x, \boldsymbol{v})\, \mathrm{d}^3\boldsymbol{v}, \tag{5.1}$$

as a measure of non-gyrotropy. Upon the shock crossing the distribution becomes non-gyrotropic and gradually gyrotropizes: the oscillations of P_{xy} damp with the distance from the shock. The gyrotropization is the slowest without overshoot (blue curve) and fastest with overshoot and unreduced potential (black curve).

6. Discussion and conclusions

The present study focuses on the role of the overshoot as a part of the self-organized shock structure. In analysing the influence of the overshoot on the ion dynamics we restricted ourselves with comparison of a model shock profile without an overshoot with the same profile and an overshoot added. Ions were traced as test particles in both

https://doi.org/10.1017/S0022377823000090 Published online by Cambridge University Press

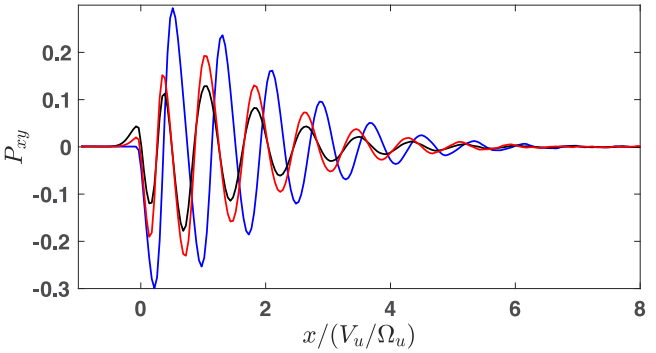

FIGURE 9. The off-diagonal pressure P_{xy} as a measure of non-gyrotropy. Blue: no overshoot. Black: overshoot and unreduced potential. Red: overshoot and reduced potential.

profiles and the resulting downstream distributions were compared. The shock parameters, including the ramp width, the overshoot width and the position of the overshoot maximum, remained fixed during the numerical analysis. Ion distributions depend on all these parameters, as well as on the shock angle, Mach number, upstream temperature and magnetic compression. All these were not varied either, since the central question was what difference the presence of an overshoot makes to the downstream ion distributions. The only parameter which was varied was the cross-shock potential: in one case with an overshoot the downstream potential was equal to the potential without an overshoot, in the other case the maximum potential at the overshoot was equal to the potential without an overshoot. It is clear that any quantitative comparison should be done with caution since the scales and the potential are not known at present. However, some clear differences were found which allow us to make conclusions about the importance of the overshoot. The main effect is ion reflection, which is absent or too weak without an overshoot. Without reflected ions the downstream distribution is under-heated, non-gyrotropy relaxation is slow and eventual anisotropy is very strong. An overshoot enhances ion reflection and, therefore, ion heating. Gyrotropization and isotropization just behind the overshoot are more efficient, due to the reflected ions. These processes are further affected by the undershoot and subsequent magnetic oscillations, as well by the time-dependent features, so that the presented values should be understood literally. Yet, the presence of a substantial population guarantees faster damping of the fluctuations of the moments of the ion distribution. Efficiency of ion reflection depends on the shock angle and the ratio $v_T/V_u = \sqrt{\beta_i/2}/M$, so that at larger θ and/or smaller β_i the effect of the overshoot may look slightly different. For example, we can expect that ion phase space holes would be observed for lower v_T/V_u. In all cases, the role of the overshoot in the self-organization of a shock structure is in adjusting the level of ion reflection as it is required for the stable transfer of the mass, momentum and energy across the part of the shock which has not arrived at the uniform state yet.

Acknowledgements

Editor Antoine C. Bret thanks the referees for their advice in evaluating this article.

Declaration of interest

The authors report no conflict of interest.

https://doi.org/10.1017/S0022377823000090 Published online by Cambridge University Press

Funding

M.G. was partially supported by NSF-BSF grant 2019744. M.G., A.D. and C.R. were partially supported by the European Union's Horizon 2020 research and innovation program under grant agreement No. 101004131 (SHARP). A.D. received financial support from the Swedish National Space Agency (Grant 2020-00111). N.P. was supported, in part, by NSF-BSF award 2010450 and NASA grant 80NSSC18K1649. N.P. was additionally supported by the *IBEX* mission as a part of NASA's Explorer program. V.R. was partially supported by NASA grant 80NSSC18K1649 and NSF-BSF award 2010144.

REFERENCES

BALE, S.D., BALE, S., MOZER, F.S., MOZER, F., HORBURY, T. & HORBURY, T.S. 2003 Density-transition scale at quasiperpendicular collisionless shocks. *Phys. Rev. Lett*. **91**, 265004.

BALE, S.D., BALIKHIN, M.A., HORBURY, T.S., KRASNOSELSKIKH, V.V., KUCHAREK, H., MÖBIUS, E., WALKER, S.N., BALOGH, A., BURGESS, D., LEMBÈGE, B., LUCEK, E.A., SCHOLER, M., SCHWARTZ, S.J. & THOMSEN, M.F. 2005 Quasi-perpendicular shock structure and processes. *Space Sci. Rev*. **118**, 161–203.

BALIKHIN, M.A., ZHANG, T.L., GEDALIN, M., GANUSHKINA, N.Y. & POPE, S.A. 2008 Venus express observes a new type of shock with pure kinematic relaxation. *Geophys. Res. Lett*. **35**, L01103.

BURCH, J.L., MOORE, T.E., TORBERT, R.B. & GILES, B.L. 2016 Magnetospheric multiscale overview and science objectives. *Space Sci. Rev*. **199** (1–4), 5–21.

BURGESS, D., HELLINGER, P., GINGELL, I. & TRÁVNÍČEK, P.M. 2016 Microstructure in two- and three-dimensional hybrid simulations of perpendicular collisionless shocks. *J. Plasma Phys*. **82**, 905820401.

COHEN, I.J., *et al.* 2019 High-resolution measurements of the cross-shock potential, ion reflection, and electron heating at an interplanetary shock by MMS. *J. Geophys. Res*. **90**, 12095

DIMMOCK, A.P., BALIKHIN, M.A., KRASNOSELSKIKH, V.V., WALKER, S.N., BALE, S.D. & HOBARA, Y. 2012 A statistical study of the cross-shock electric potential at low Mach number, quasi-perpendicular bow shock crossings using Cluster data. *J. Geophys. Res*. **117**, 02210.

ESELEVICH, V.G., ES'KOV, A.G., KURTMULLAEV, R.K. & MALYUTIN, A.I. 1971 Isomagnetic discondinuity in a collisionless shock wave in a plasma. *Sov. J. Exp. Theor. Phys. Lett*. **13**, 49.

FARRIS, M.H. & RUSSELL, C.T. 1994 Determining the standoff distance of the bow shock: Mach number dependence and use of models. *J. Geophys. Res*. **99**, 17.

FARRIS, M.H., RUSSELL, C.T. & THOMSEN, M.F. 1993 Magnetic structure of the low beta, quasi-perpendicular shock. *J. Geophys. Res*. **98**, 15.

FIUZA, F., SWADLING, G.F., GRASSI, A., RINDERKNECHT, H.G., HIGGINSON, D.P., RYUTOV, D.D., BRUULSEMA, C., DRAKE, R.P., FUNK, S., GLENZER, S., GREGORI, G., LI, C.K., POLLOCK, B.B., REMINGTON, B.A., ROSS, J.S., ROZMUS, W., SAKAWA, Y., SPITKOVSKY, A., WILKS, S. & PARK, H.-S. 2020 Electron acceleration in laboratory-produced turbulent collisionless shocks. *Nat. Phys*. **16**, 916–920.

GEDALIN, M. 2016 Transmitted, reflected, quasi-reflected, and multiply reflected ions in low-Mach number shocks. *J. Geophys. Res*. **121**, 10.

GEDALIN, M. 2019*a* Kinematic collisionless relaxation and time dependence of supercritical shocks with alpha particles. *Astrophys. J*. **880**, 140.

GEDALIN, M. 2019*b* Kinematic collisionless relaxation of ions in supercritical shocks. *Front. Phys*. **7**, 692.

GEDALIN, M. & GANUSHKINA, N. 2022 Implications of weak rippling of the shock ramp on the pattern of the electromagnetic field and ion distributions. *J. Plasma Phys*. **88**, 905880301.

GEDALIN, M., POGORELOV, N.V. & ROYTERSHTEYN, V. 2021 Boundary conditions at the heliospheric termination shock with pickup ions. *Astrophys. J*. **916**, 57.

HAGGERTY, C.C., BRET, A. & CAPRIOLI, D. 2021 Kinetic simulations of strongly magnetized parallel shocks: deviations from MHD jump conditions. *Mon. Not. R. Astron. Soc*. **509**, 2084–2090.

Hanson, E.L.M., Agapitov, O.V., Mozer, F.S., Krasnoselskikh, V., Bale, S.D., Avanov, L., Khotyaintsev, Y. & Giles, B. 2019 Cross-shock potential in rippled versus planar quasi-perpendicular shocks observed by MMS. *Geophys. Res. Lett*. **46**, 2381–2389.

Hobara, Y., Balikhin, M., Krasnoselskikh, V., Gedalin, M. & Yamagishi, H. 2010 Statistical study of the quasi-perpendicular shock ramp widths. *J. Geophys. Res*. **115**, 11106.

Iapichino, L. & Brüggen, M. 2012 Magnetic field amplification by shocks in galaxy clusters: application to radio relics. *Mon. Not. R. Astron. Soc*. **423**, 2781–2788.

Kennel, C.F. 1988 Shock structure in classical magnetohydrodynamics. *J. Geophys. Res*. **93**, 8545–8557.

Krasnoselskikh, V., Balikhin, M., Walker, S.N., Schwartz, S., Sundkvist, D., Lobzin, V., Gedalin, M., Bale, S.D., Mozer, F., Soucek, J., Hobara, Y. & Comişel, H. 2013 The dynamic quasiperpendicular shock: cluster discoveries. *Space Sci. Rev*. **178**, 535–598.

Krasnoselskikh, V.V., Lembège, B., Savoini, P. & Lobzin, V.V. 2002 Nonstationarity of strong collisionless quasiperpendicular shocks: theory and full particle numerical simulations. *Phys. Plasmas* **9**, 1192–1209.

Kurtmullaev, R.K., Malinovskii, V.K., Nesterikhin, Y.E. & Ponomarenko, A.G. 1966 Excitation of strong collisionless shock waves in a plasma. *J. Appl. Mech. Tech. Phys*. **6**, 68–73.

Lalti, A., Khotyaintsev, Y.V., Dimmock, A.P., Johlander, A., Graham, D.B. & Olshevsky, V. 2022 A database of MMS bow shock crossings compiled using machine learning. *J. Geophys. Res*. **127**, JA030454.

Lowe, R.E. & Burgess, D. 2003 The properties and causes of rippling in quasi-perpendicular collisionless shock fronts. *Ann. Geophys*. **21**, 671–679.

Medvedev, M.V., Silva, L.O. & Kamionkowski, M. 2006 Cluster magnetic fields from large-scale structure and galaxy cluster shocks. *Astrophys. J*. **642**, L1–L4.

Morse, D.L. 1973 Electrostatic potential rise across perpendicular shocks. *Plasma Phys*. **15**, 1262–1264.

Newbury, J.A., Russell, C.T. & Gedalin, M. 1998 The ramp widths of high-Mach-number, quasi-perpendicular collisionless shocks. *J. Geophys. Res*. **103**, 29581–29594.

Niemann, C., Gekelman, W., Constantin, C.G., Everson, E.T., Schaeffer, D.B., Bondarenko, A.S., Clark, S.E., Winske, D., Vincena, S., Van Compernolle, B. & Pribyl, P. 2014 Observation of collisionless shocks in a large current-free laboratory plasma. *Geophys. Res. Lett*. **41**, 7413–7418.

Ofman, L., Balikhin, M., Russell, C.T. & Gedalin, M. 2009 Collisionless relaxation of ion distributions downstream of laminar quasi-perpendicular shocks. *J. Geophys. Res*. **114** (A), 09106.

Ofman, L. & Gedalin, M. 2013 Rippled quasi-perpendicular collisionless shocks: local and global normals. *J. Geophys. Res*. **118**, 5999–6006.

Omidi, N., Desai, M., Russell, C.T. & Howes, G.G. 2021 High Mach number quasi-perpendicular shocks: spatial versus temporal structure. *J. Geophys. Res*. **126**, e2021JA029287.

Pollock, C., *et al.* 2016 Fast plasma investigation for magnetospheric multiscale. *Space Sci. Rev*. **199**, 331–406.

Pope, S.A. 2020 A survey of venus shock crossings dominated by kinematic relaxation. *J. Geophys. Res*. **125**, A028256.

Pope, S.A., Gedalin, M. & Balikhin, M.A. 2019 The first direct observational confirmation of kinematic collisionless relaxation in very low Mach number shocks near the earth. *J. Geophys. Res*. **165**, 3–15.

Russell, C.T., *et al.* 2016 The magnetospheric multiscale magnetometers. *Space Sci. Rev*. **199**, 189–256.

Schaeffer, D.B., Winske, D., Larson, D.J., Cowee, M.M., Constantin, C.G., Bondarenko, A.S., Clark, S.E. & Niemann, C. 2017 On the generation of magnetized collisionless shocks in the large plasma device. *Phys. Plasmas* **24**, 041405.

Schwartz, S.J., Ergun, R., Kucharek, H., Wilson, L., Chen, L.-J., Goodrich, K., Turner, D., Gingell, I., Madanian, H., Gershman, D. & Strangeway, R. 2021 Evaluating the de Hoffmann-Teller cross-shock potential at real collisionless shocks. *J. Geophys. Res*. **126**, A029295.

Schwartz, S.J., Thomsen, M.F., Bame, S.J. & Stansberry, J. 1988 Electron heating and the potential jump across fast mode shocks. *J. Geophys. Res*. **93**, 12923–12931.

SCKOPKE, N., PASCHMANN, G., BAME, S.J., GOSLING, J.T. & RUSSELL, C.T. 1983 Evolution of ion distributions across the nearly perpendicular bow shock - specularly and non-specularly reflected-gyrating ions. *J. Geophys. Res.* **88**, 6121–6136.

SIMIONESCU, A., ROEDIGER, E., NULSEN, P.E.J., BRÜGGEN, M., FORMAN, W.R., BÖHRINGER, H., WERNER, N. & FINOGUENOV, A. 2009 The large-scale shock in the cluster of galaxies Hydra A. *Astron. Astrophys*. **495**, 721–732.

WILSON, L.B., CHEN, L.-J. & ROYTERSHTEYN, V. 2021 The discrepancy between simulation and observation of electric fields in collisionless shocks. *Front. Astron. Space Sci*. **7**, 592634.

YAO, W., *et al.* 2022 Detailed characterization of a laboratory magnetized supercritical collisionless shock and of the associated proton energization. *Matter Radiat. Extrem*. **7**, 014402.

https://doi.org/10.1017/S0022377823000090 Published online by Cambridge University Press